Hindawi
Advances in Civil Engineering
Volume 2023, Article ID 6374897, 15 pages
https://doi.org/10.1155/2023/6374897

Research Article

Mechanical Properties of Improved Multiple-Layers Viscoelastic Damper

Joaquim Mimusse Tchamo, Yi Xiao, and Ying Zhou

State Key Laboratory of Disaster Reduction in Civil Engineering, Tongji University, Shanghai, China

Correspondence should be addressed to Ying Zhou; yingzhou@tongji.edu.cn

Received 8 December 2022; Revised 30 July 2023; Accepted 8 August 2023; Published 25 September 2023

Academic Editor: Angelo Aloisio

Copyright © 2023 Joaquim Mimusse Tchamo et al. This is an open access article distributed under the Creative Commons Attribution License, which permits unrestricted use, distribution, and reproduction in any medium, provided the original work is properly cited.

Viscoelastic dampers (VEDs) have been implemented successfully to reduce structural vibrations due to earthquakes and wind events. Conventional VEDs consist of two viscoelastic (VE) layers chemically bounded at their entire contact surface to three steel plates. This configuration has proven to be efficient in controlling the structure vibration. It has also been reported that VEDs can dissipate energy at any level of vibration, producing damping forces. However, when very large damping forces are required, the shear area of the VE layers and the steel plates should be increased to reach the target damping force since the energy is dissipated by hysteretic shear deformation developed in the VE material. Two main issues are associated with this large area. First, the steel plates are more susceptible to experiencing buckling due to out-of-plane deformations. Second, the overall size of the damper becomes larger which is not desirable from the architectural perspective and sometimes from the space usage perspective. As a solution, this study proposes an innovative VED so-called multiple-layers viscoelastic damper (MLVED) able to produce larger damping forces. The proposed MLVED consists of four VE layers bounded between five steel plates. The dynamic mechanical properties of MLVED are initially investigated through a full-scale test. With the test results, the finite element model is developed and calibrated using the commercial software ABAQUS. At a later stage, the calibrated model was used to investigate numerically the mechanical performance of MLVED if different VE layers areas and thicknesses are considered. Results indicated that the proposed MLVED possesses good energy dissipation capacity and its mechanical properties are strongly influenced by strain amplitude rather than loading frequency. Numerical results also showed that the damper is effective in dissipating energy even if different VE layers areas and thicknesses are considered. However, an optimal combination between the area and thickness of the VE layers needs to be found to maximize the damper performance.

1. Introduction

Past earthquakes and strong wind events have proven to be very threatening to the integrity of different types of structures bringing tremendous economic losses and deaths of people [1, 2]. Protecting the structures against such hazards by controlling the lateral structure vibration is required [3–5]. Recently, several protective systems have been developed and applied including passive, active, semiactive, and hybrid control systems [6–8].

Passive control systems are known as one of the most preferable solutions due to their advantages such as no need of electrical energy to work, simple design, construction, maintenance, easy installation, and low cost [9, 10]. Viscoelastic dampers (VEDs) are very popular among passive energy dissipation devices. They can dissipate energy at any level of vibration and thus are an effective solution if both wind and earthquake hazards have to be considered [11].

Although the first application of VEDs for structural control date back to 1960 when more than 10,000 VEDs were applied in each tower of the World Trade Center in New York, the first relevant published study on the application of these devices for vibration reduction was performed on 1972 by Keel and Mahmoodi [12]. In his study, he investigated and established the properties of viscoelastic (VE) materials through an extensive experimental program.

Many other studies were performed from that period up to date. Keel and Mahmoodi [12] and Mahmoodi and

Keel [13] designed and evaluated the performance of VEDs for suppression of wind-induced sway of Columbia Centre Building. The first studies on the application of VEDs for seismic vibration reduction were performed by Chang et al. [14]. They investigated the behavior of 2/5-scale five-story steel with added VEDs under strong ground motions through a shaking table. They designed three types of VEDs distinguished by dimensions and VE materials.

The mechanical properties of VEDs were investigated by Xu et al. [15], Chen et al. [16], Han et al. [17], and Xu et al. [18]. During their studies, they designed and manufactured different VEDs varying in size and VE materials. All the specimens were subjected to different loading conditions considering the variation in stain amplitude, frequency vibration, and the number of cycles. The mechanical properties of the VEDs were computed from the hysteretic curves and lately used to simulate the behavior of the dampers through several existing mechanical models.

Over the years, innovative damping systems combining the advantages of VEDs and other devices were introduced. A new system to increase the level of inherent damping of tall coupled shear wall buildings under earthquake-induced and wind-induced vibrations was introduced in a study performed by Montgomerey and Christopoulos [19]. This system called viscoelastic coupling dampers adds high-damping elements in place of reinforced concrete coupling beams and thus does not require any additional usable architectural space. If well-designed and installed in high-rise buildings, they are very effective in controlling the structure for all modes of vibration. Shu et al. [20] developed an innovative type of replaceable moment-resisting viscoelastic damper to improve the behavior of steel frame buildings under wind and earthquake loads. The innovative system has the advantage of being installed in the lieu of existing steel moment connections, which does not require additional architectural space. Another advantage of the proposed system is that the sacrificial fuse segment can be easily replaced after an earthquake if the interstory drift exceeds a predefined threshold.

An experimental study of a brace-type VED under long-period and long-duration excitation was performed by Osabel et al. [21]. From the tests, they found that under long-period the damper temperature increases significantly causing the damper properties to reduce by more than 40%. They also found that under long-duration harmonic loading such as strong winds, despite the drastic decrease of the damper properties due to the several loading cycles, the damper eventually reached steady-state behavior. In this state, the damper properties became constant.

More recently Fang et al. [22] introduced a new hybrid self-centering damping system, which the objective was to suppress the limitations of the current existing self-centering damping systems. In their study, the proposed to incorporate shape memory alloy elements combined with VED aiming to control the vibration of building structures. From their results, they concluded that to reach a moderate damping ratio in peak and residual deformation control is highly effective to use of VE material. At the final stage, they proposed design recommendations to implement the introduced device. A replaceable rotational VEDs for improving structural damping and resilience of steel frames was proposed by Shu et al. [20]. They used a sacrificial fuse segment in combination with replaceable rotational VEDs to protect the structure at large interstory drifts. In their study, they also proposed a low-damage solution for the floor diaphragm with replaceable rotational VEDs. Results indicated that the proposed replaceable rotational VEDs improved the system damping and reduced the earthquake-induced roof acceleration and the peak interstory drift by up to 30%.

Qian et al. [23] proposed and investigated an innovative pretensioned shape memory alloy cable combined with a novel self-centering VED to enhance the initial stiffness and self-centering capability of VED, so-called self-centering high-damping rubber damper. In their study, they investigated both experimentally and numerically the influence of initial strain, loading amplitude, and strain rate on the behavior of shape memory alloy cables after training and pretensioning. From the results, they concluded that compared with traditional VED, the proposed self-centering high-damping rubber damper has better initial stiffness and self-centering capacities. A novel lead-VE coupling beam damper was proposed by Fang et al. [24]. The proposed damping system which is not only independent of the loading frequency, but also has better fatigue performance with good energy dissipation capacity, was numerically and experimentally investigated and discussed. Experimental results indicated that the lead-VE coupling beam damper showed a favorable deformation capability, frequency-independent performance, fatigue resistance, and stable energy dissipation capacity under cyclic loading.

As discussed before, VEDs have been exhaustively investigated over the years. However, the majority of them have considered the traditional two rectangular VE layers bounded between three rectangular steel plates. Additionally, although VE coupling beams (which combine several layers of VE material) have been extensively investigated, no record of using VEDs with four layers (to be mounted in conventional bracing systems) to increase the damping forces to be transferred to the frame structure has been found by the author at the time of the present study. Finally, very few experimental studies have been performed on full-scale VEDs due to the challenge presented by many laboratory facilities to reach high values of loading forces at higher frequencies.

Aiming to overcome these limitations, this study proposes an innovative VED so-called multiple-layers viscoelastic damper (MLVED) able to produce large damping forces with relatively small size. The dynamic mechanical properties of MLVED are initially investigated through full-scale tests and numerically at a later stage.

2. Description of the Proposed Damper MLVED

In this section, the innovative MLVED is introduced. The proposed MLVED consists of four rectangular VE layers bounded between five rectangular steel plates, two outer plates, and three at the center instead of the traditional two rectangular VE layers bounded between three rectangular

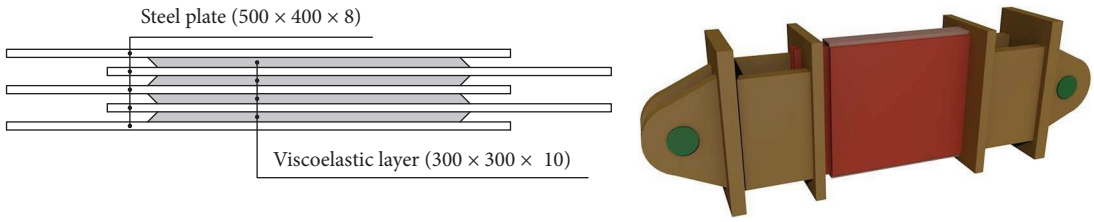

(a) (b)

Figure 1: Schematic drawing of MLVED: (a) inner section and (b) 3D assembled MLVED.

steel plates. This modification aims to increase the damping force produced by a traditional VED. In addition, the proposed MLVED is reinforced with a *U*-shaped steel profile connecting the two outer plates at the top and bottom. The goal is to prevent any buckling of the steel plates due to out-of-plane deformation when the compression force is applied to the damper. With the same goal, the center steel plates are also reinforced from the outside using four stiffeners on each plate. This damper dissipates energy through the shear deformation of the VE layers. In Figure 1, the schematic diagram of the proposed MLVED is depicted.

3. Methodology and Theory of MLVED Performance Test

VEDs are generally subjected to alternating loads, which can be described by a series of sine function combinations. For this reason, in the present study, sinusoidal waveform excitations were applied to evaluate the mechanical properties of the proposed MLVED.

Under the sinusoidal wave loading with a frequency ω, the relationship of shear stress and shear strain for a VE material is given as follows [25]:

$$\varepsilon(t) = \varepsilon_0 \sin \omega t, \tag{1}$$

$$\sigma(t, \omega) = \sigma_0 \sin(\omega t + \delta), \tag{2}$$

where $\varepsilon(t)$, $\sigma(t, \omega)$, and δ are shear strain, shear stress, and phase difference, respectively. ε_0 and σ_0 represent peak strain and peak stress, respectively. Equation (2) can be expanded as follows:

$$\begin{aligned} c\sigma(t, \omega) &= \sigma_0 \sin \omega t \cos \delta + \sigma_0 \cos \omega t \sin \delta \\ &= \varepsilon_0 [E'(\omega) \sin \omega t + E''(\omega) \cos \omega t], \end{aligned} \tag{3}$$

where $E'(\omega) = (\sigma_0/\varepsilon_0) \cos \delta$ and $E''(\omega) = (\sigma_0/\varepsilon_0) \sin \delta$ are storage modulus and loss modulus of VE material, respectively. The storage modulus E'' represents the work done by the stress in phase with the strain, which is converted into energy and stored in the sample, and the energy of this part can make its elastic deformation recover. The loss modulus represents the energy lost by the transformation into heat during deformation. The ratio of loss modulus and storage modulus is the loss factor η of VE material and is given as follows:

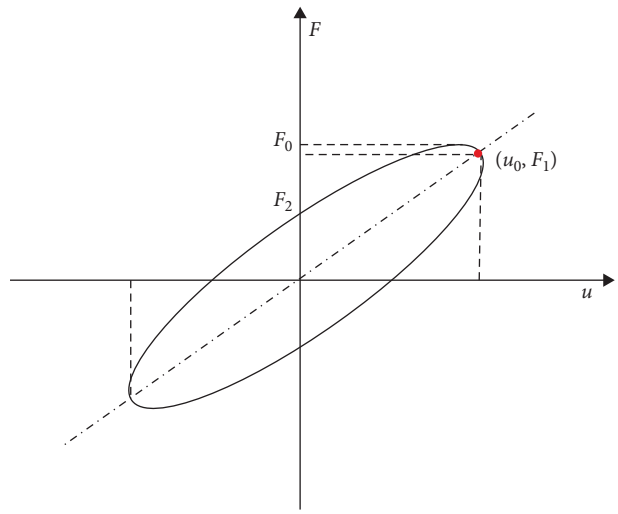

Figure 2: Typical force–deformation curve.

$$\eta = \frac{E''}{E'} = \tan \delta. \tag{4}$$

Introducing Equation (1) into Equation (3) and considering that $\sin^2 \omega t + \cos^2 \omega t = 1$ then the following equation is obtained as follows:

$$\left(\frac{\sigma(t, \omega) - E''(\omega)\varepsilon(t)}{\varepsilon_0 E''(\omega)}\right)^2 + \left(\frac{\varepsilon(t)}{\varepsilon_0}\right)^2 = 1. \tag{5}$$

Based on the above analysis, the relationship between force F and displacement μ of VED follows Equation (5), which is in the form of an elliptic equation and can also be given as follows:

$$\left(\frac{F - K_{d1}\mu}{\eta K_{d1}\mu_0}\right)^2 + \left(\frac{\mu}{\mu_0}\right)^2 = 1, \tag{6}$$

where F is the damping force, K_{d1} is the energy storage stiffness of the damper, μ is the excitation displacement, and μ_0 is the maximum displacement of the damper.

During the VED test, the loading displacement and loading frequency are controlled, and the corresponding loading force is obtained from the test facility in the form of hysteretic curves as depicted in Figure 2. The dynamic mechanical

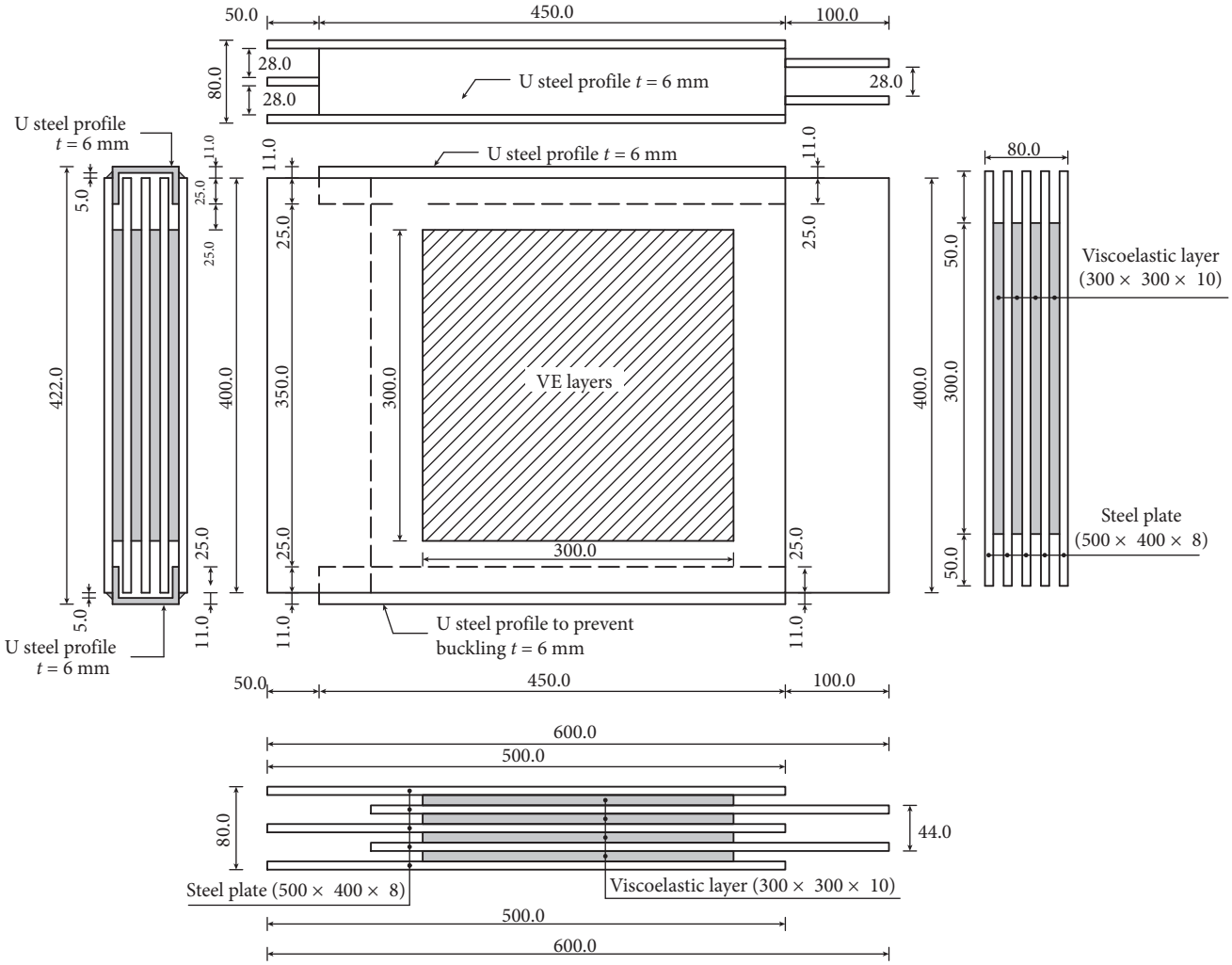

Figure 3: Dimensions of the specimen.

properties of the VED are evaluated by computing from those curves the storage modulus G_1, the loss modulus G_2, the loss factor η, and the energy dissipation E_d through the following equations:

$$G_1 = \frac{F_1 \cdot h_v}{n_v \cdot A_v \cdot \mu_0}, \tag{7}$$

$$\eta = \frac{F_2}{F_1}, \tag{8}$$

$$G_2 = \eta G_1, \tag{9}$$

where F_1 is the corresponding force at displacement μ_0, F_2 is the corresponding force at zero displacement ($F_2 = \eta K_{d1} \mu_0$), n_v, h_v, and A_v are the number, the shear thickness, and the shear area of the VE layers, respectively.

The performance of VED is usually expressed by storage stiffness K_{d1}, equivalent damping C_e, and single energy consumption E_d, given as follows [26]:

$$K_{d1} = \frac{n_v \cdot G_1 \cdot A_v}{h_v}, \tag{10}$$

$$C_e = \frac{n_v \cdot G_2 \cdot A_v}{\omega h_v}, \tag{11}$$

$$E_d = n_v \cdot \pi \cdot G_2 \cdot A_v \cdot \mu_0^2 / h_v. \tag{12}$$

The previous equations are very simple analytical expressions that relate loading to material mechanical properties using simplified models and thus adopted by many design codes to process the data on VEDs. Therefore, in the present study, the evaluation of the mechanical properties of the proposed MLVED is performed using those equations.

4. Experimental Test Program and Results

4.1. Test Specimens. One MLVED was designed and manufactured, and its dimensions are shown in Figure 3. All the steel parts were materialized using Q345 steel, one kind of Chinese standardized mild steel with a yield strength of 345 MPa. The damper consisted of four VE layers of

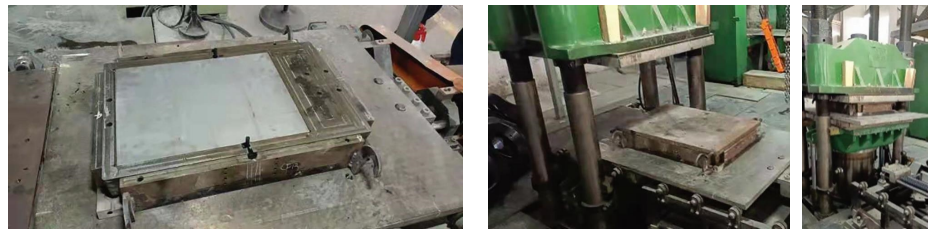

(a) (b)

Figure 4: Vulcanization process: (a) assembly of the VE layers, steel plates, and mold; (b) flat vulcanizing machine.

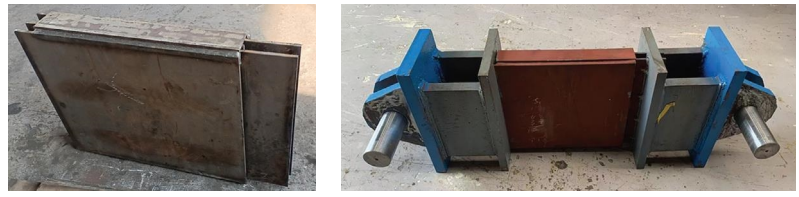

(a) (b)

Figure 5: Manufactured specimen: (a) before welding the connectors and (b) after welding the connectors.

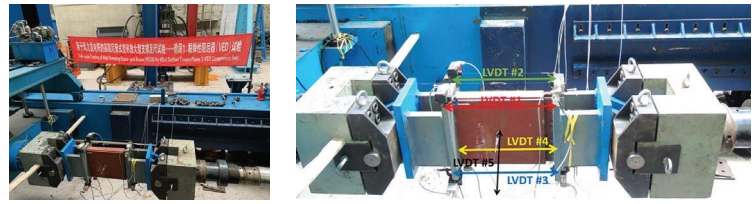

(a) (b)

Figure 6: Test setup: (a) loading machine and (b) instrumentation.

300 × 300 mm bounded between five steel plates of 500 × 400 mm in area. The thickness of the VE layers and the steel plates were 10 and 8 mm, respectively. The VE material used for the test specimen is composed of smoked sheet rubber, styrene-butadiene rubber, viscosifying resin, carbon black, naphthenic oil, nanozinc oxide, activator, antioxidant, anticoke agent, microcrystalline wax, accelerant, and sulfur. The proportion of each element is regarded as intellectual property by the manufacturer company. The process of production of VE materials comprises three main stages including plasticization, mixing, and vulcanization. The main objective of plasticizing is to alter the rheological properties of rubber, enlarge the plasticity, decrease the viscosity, and make it compatible with several additives during the mixing stage. The main purpose of mixing is to combine the plastic rubber or raw rubber and compounding agent in order to have them dispersed.

The vulcanization process which consists of bounding between the VE pads and the steel plates was materialized by a vulcanizing machine (shown in Figure 4) in which the mold with VE material and the steel plate was put inside the vulcanizing machine set to a determined vulcanization condition (temperature: 160°C, time: 15 min, and pressure: 10 MPa) to ensure the perfect adhesion between the two materials.

Stiffeners were used to ensure the shear deformation of the VE layers preventing any out-of-plane deformation. Two *U*-shaped profiles are welded at the top and bottom of the outer steel plates and eight triangular stiffeners were welded on the inner plates. Precisely designed connectors were welded to both ends of MLVEDs in order to allow their installation on the loading facility. In Figures 5(a) and 5(b), the MLVED before and after welding the connectors are depicted, respectively.

4.2. Test Setup (Loading Machine). In the present study, the dynamic mechanical property tests on MLVED were carried out on a 2,000 kN high-speed electrohydraulic servo actuator as depicted in Figure 6(a). The specimen was installed on the loading machine through the specially designed connectors as shown in Figure 5. Horizontal cyclic controlled loads were applied to the specimen and the maximum recorded force and displacement were 800 kN and 30 mm on a frequency range from 0.1 to 4.0 Hz.

The ambient temperature in the room facility was kept at 25–30°C with no consideration of the influence of temperature variation. Thus, the study only considered the effects of loading frequency and strain amplitude on the properties of the MLVED.

The loads and displacements applied by the loading machine were recorded by the built-in acquisition system of the machine. To ensure the accuracy of the results, five linear

Table 1: Loading protocol.

Content	Frequency (Hz)	Strain amplitude (%)	Cycles
Different strain amplitude	1.0	25, 50, 75, 100, 125, 150, 200 250, 300	5
Different loading frequencies	0.1, 0.5, 1.0, 2.0, 4.0	100	5
Fatigue test	1.0	100	30

variable differential transducers (LVDTs) were installed on the specimen as indicated in Figure 6(b) to capture the applied displacement. LVDTs #1, #2, #3, and #4 measured the nominal damper deformation while LVDT #5 controlled the out-of-plane displacement of the specimen.

4.3. Loading Protocol. The applied loading protocol follows the recommendation prescribed in the standard for dampers for vibration energy dissipation of buildings (JG/T 209-2012) [27] for testing VEDs. Displacements in the form of the sinusoidal wave were used and five cycles were repeated for each amplitude. To investigate the effect of loading frequency and strain amplitude on the mechanical behavior of MLVED, as well as the antifatigue performance, three different loading protocols were applied. In the first loading protocol, six loading frequencies ranging from 0.1 to 4.0 Hz were used for the same strain amplitude (100%). The second case adopted nine strain amplitudes ranging from 25% to 300% for a constant frequency of 1.0 Hz. Finally, for the last case, a shear strain amplitude of 100% was kept constant while 30 repeated cycles were applied. In Table 1, all adopted loading protocols are summarized.

4.4. Experimental Results. As mentioned in the previous section, the storage modulus, loss modulus, and loss factor are the most important parameters reflecting the dynamic mechanical properties of the MLVED and they can be computed from the tested hysteretic curves using Equations (7)–(12). In addition, the equivalent stiffness and damping also characterize the mechanical properties of the MLVED. The variation of those properties is discussed in this section.

A MATLAB program based on the previously mentioned equations was used and the obtained results are discussed considering the effect of loading frequency and strain amplitude on the mechanical behavior of MLVED, as well as the antifatigue performance.

4.4.1. Effect of Loading Frequency on the Mechanical Properties of MLVED. Figure 7 shows the hysteretic curve for MLVED with a constant strain amplitude of 100% and at six different frequencies. From the curves, it can be observed that the enveloping area and the slope of hysteresis remain almost the same, which indicates that the MLVED is frequency independent. This frequency independence is explained by the chemical composition of the resin content which results in a VE material with stable properties regardless of the frequency variation. However, slight differences in maximum stresses were recorded due to some imprecision of the loading machine when setting the strain amplitude limits in the two loading directions.

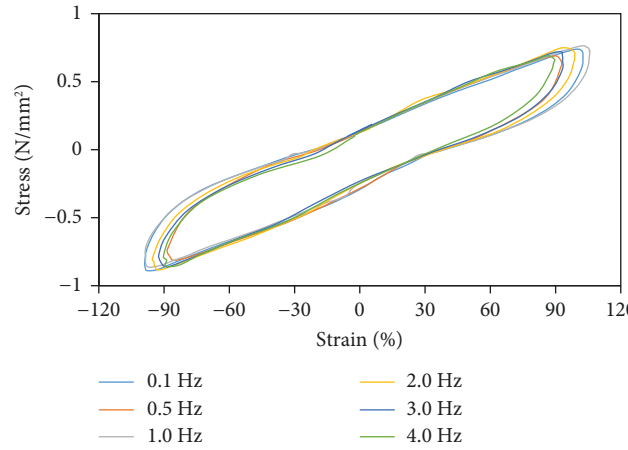

Figure 7: Frequency dependency: hysteresis curves of the MLVED at different frequencies.

Figure 8 shows the shear storage modulus, shear energy dissipation modulus, and the loss factor of the MLVED. It can be seen that no significant variation occurs on those properties when the frequency changes, confirming that this device is frequency independent. Similarly, the equivalent damping and equivalent stiffness remained almost constant for different loading frequencies as depicted in Figure 9.

4.4.2. Effect of Strain Amplitude on the Mechanical Properties of MLVED. Figure 10 shows the hysteretic curve of MLVED at different strain amplitudes for the same frequency. All the curves are full and well-shaped indicating good energy dissipation capacity at all strain ranges. The slope and enveloping area increased obviously with the increase of strain amplitude showing that the MLVED is highly strain dependent. It is also observed that the curves of the damper are ellipse shaped for strain amplitudes less than 80%, which is typical for VEDs. When the shear strain is greater than 80%, the curves change into an inverse *S*-shape. The reason is the hardening of the VE material that starts at this strain amplitude and the pinching effect under larger deformation, which is typical for nonlinear VE material. Figure 11 shows the shear storage modulus, shear loss modulus, and the loss factor of the MLVED. It can be observed that those properties are affected by the strain amplitude, especially for amplitudes less than 100%. A stable behavior is observed for amplitudes greater than 150%. The same behavior is observed for equivalent damping and equivalent stiffness as depicted in Figure 12.

4.4.3. Antifatigue Performance of MLVED. Figure 13 gives the antifatigue performance of MLVED. As recommended

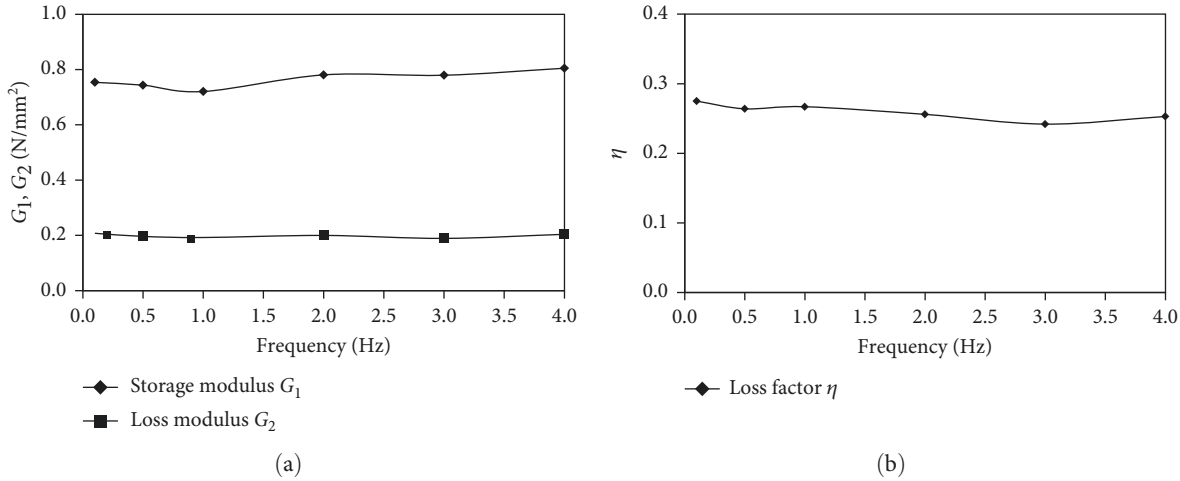

Figure 8: Frequency dependency: (a) storage modulus, loss modulus and (b) loss factor.

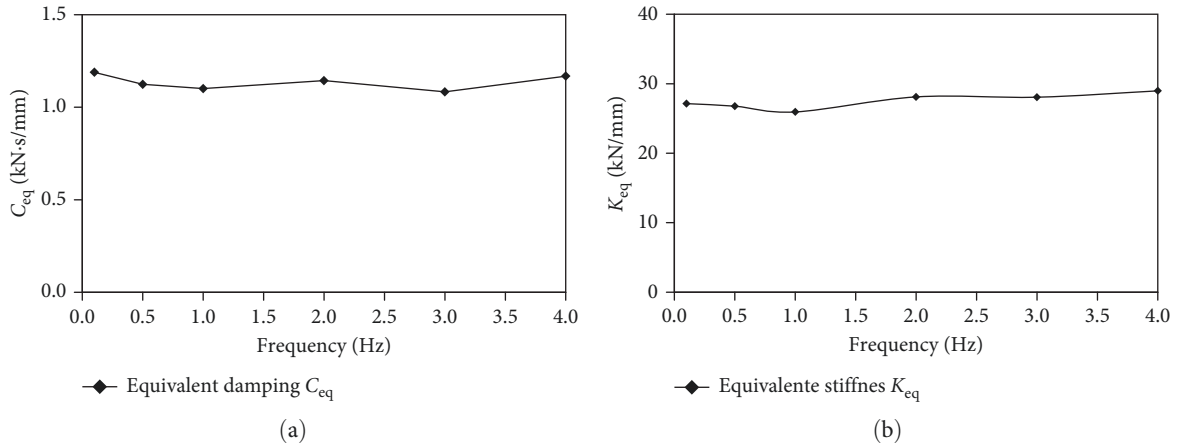

Figure 9: Frequency dependency: (a) equivalent damping and (b) equivalent stiffness.

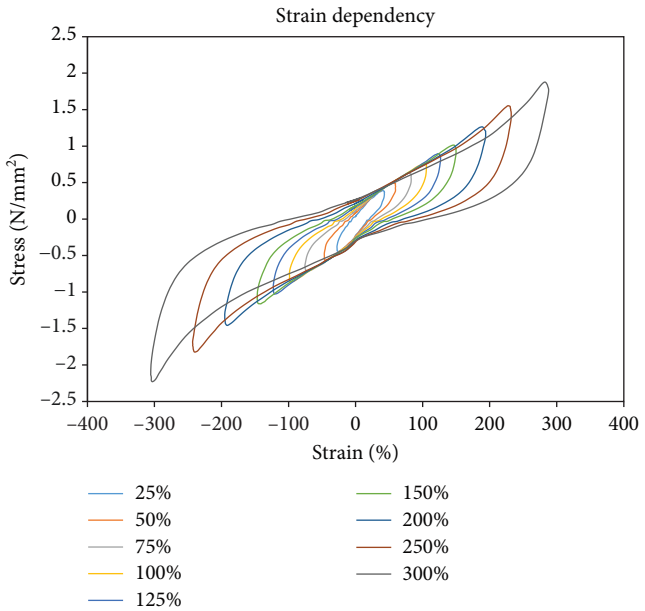

Figure 10: Strain dependency: hysteresis curves of the MLVED at different strain amplitudes.

by the standard for dampers for vibration energy dissipation of buildings (JG/T 209-2012) [27] the hysteretic curve of the third cycle is indicated as the standard to evaluate the mechanical properties of the specimens. It is required that the mechanical properties of the damper should not decrease by more than 15% after 30-cycle loading under the same designed strain amplitude. In the present study, 30 cycles of loading were applied under 1.0 Hz loading frequency for an amplitude of 10 mm. The figure shows a stable behavior although slight deterioration of the mechanical was observed. The reason is the self-heating of the VE material indicating that the proposed MLVED is sensitive to the temperature. Maximum damping force, shear storage modulus, shear energy dissipation modulus, and the loss factor of the MLVED at the third cycle are compared with those at the 30th cycle, and results are presented in Table 2. It can be seen that the reduction of damping force, shear storage modulus, shear energy dissipation modulus, and the loss factor after 30 cycles is about 8.31%, 7.30%, 12.92%, and 6.25%, respectively, which is in good agreement with what is prescribed by the standard for dampers for vibration energy dissipation of building (JG/T 209-2012) [27].

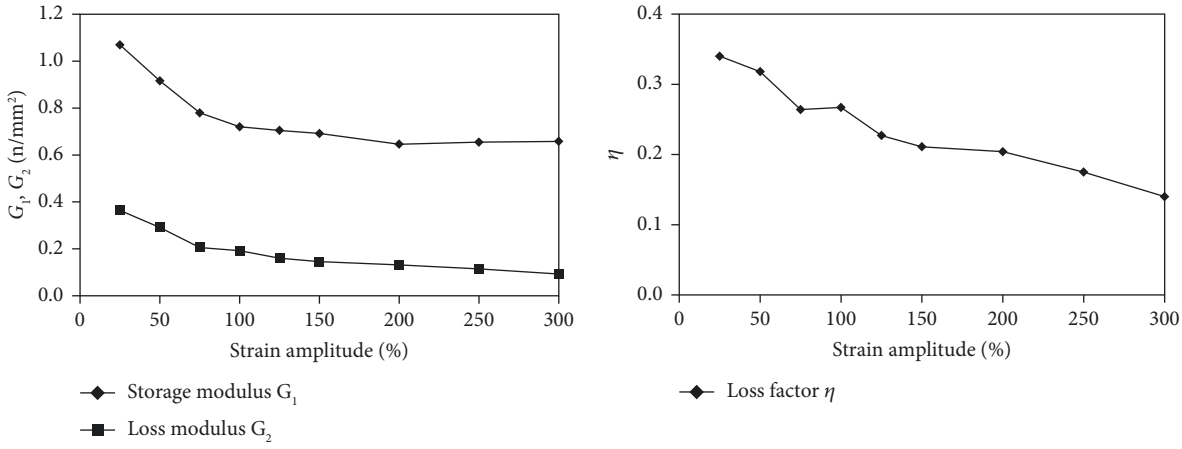

Figure 11: Strain dependency: (a) storage modulus, loss modulus and (b) loss factor.

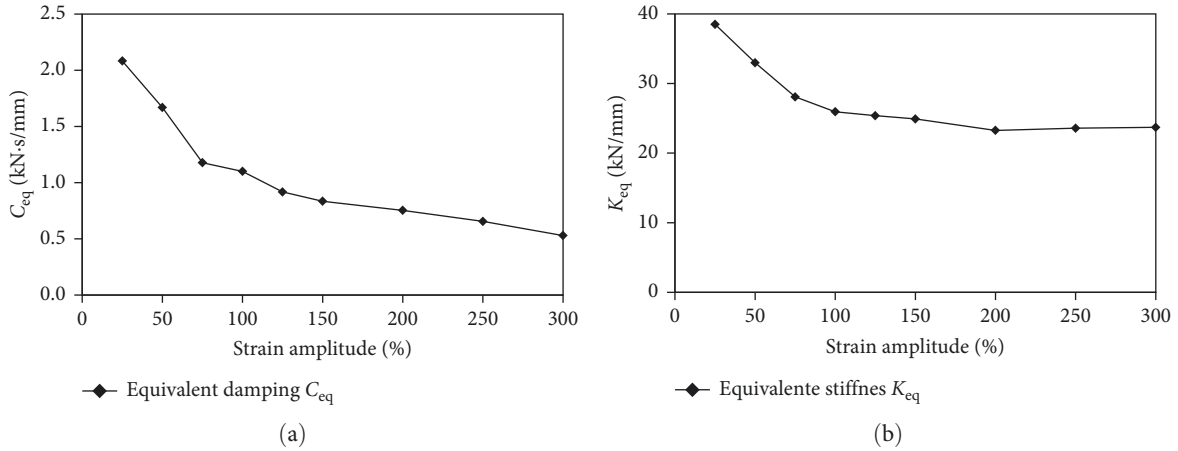

Figure 12: Strain dependency: (a) equivalent damping and (b) equivalent stiffness.

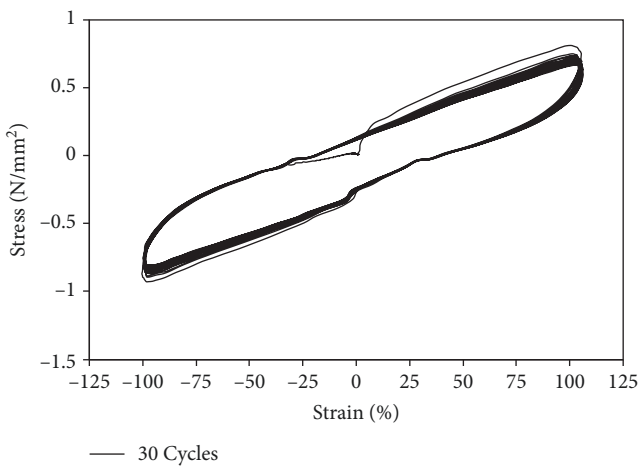

Figure 13: Antifatigue performance: hysteresis curves of the MLVED after 30 cycles.

5. Numerical Simulations of MLVED

To verify the experimental results, the finite element model of the specimen shown in Figure 14 was created using the ABAQUS/Standard analysis module [28]. The model created is similar to the specimen tested having exactly the same dimensions. The steel parts were modeled using the eight-node linear hexahedron elements with reduced integration (C3D8R). The VE layers were modeled using eight-node hybrid hexahedron elements (C3D8H) assuming that the rubber is an incompressible and isotropic material. The sweeping technique and advancing font algorithm were used to mesh the parts. The contact surfaces between the VE layers and the steel plates were modeled as tie constraints. Three steel plates of the model were completely fixed, and the two middle plates were coupled with a reference point RP-1. This reference point was subjected to step-by-step incremental cyclic displacement along the longitudinal directions of the plates.

Table 2: Antifatigue performance of MLVED.

Content	3rd Cycle	30th Cycle	Difference (%)
Damping force (kN)	318.7	292.23	8.31
Shear storage modulus (G_1)	0.7365	0.6827	7.30
Shear energy dissipation modulus (G_2)	0.1883	0.1639	12.96
Loss factor (η)	0.256	0.24	6.25
Average			8.70

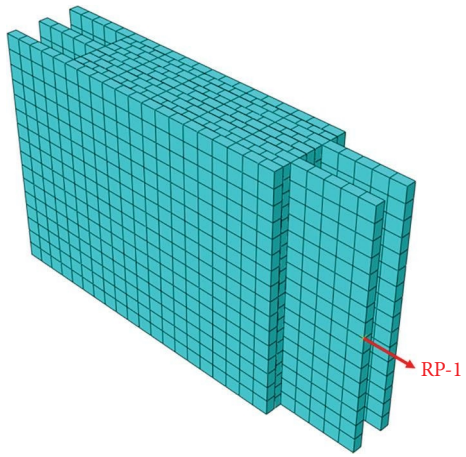

Figure 14: Finite element model of the specimen.

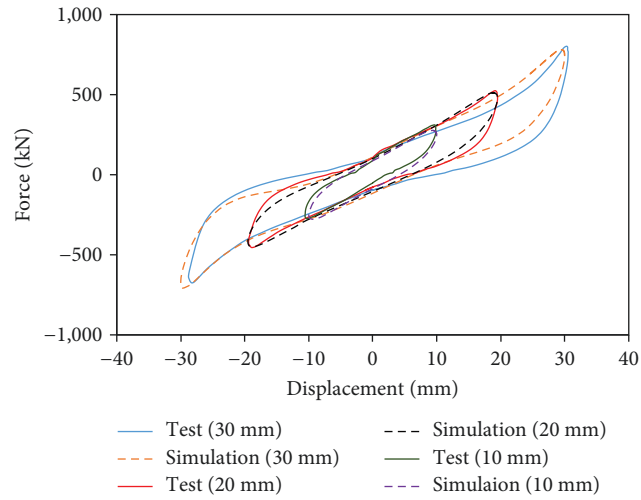

Figure 15: Comparison between the test curves and the simulation curves.

Table 3: Parameters for modeling rubber material.

Constitutive model	Fitting parameters	
Hyperelastic (Moone–Rivlin model)	C_{10}	0.58
	C_{01}	0.035
	D_1	0
Yeon	C_{10}	0.35
	C_{20}	−0.0042
	D_{30}	0.001
Viscoelastic	*g–i Prony*	0.79
	k–i Prony	0
	tau–i Prony	0.0685

During the analysis, the loading protocol used was the same as the specimens' full-scale tests.

5.1. Definition of Material Properties. The rubber material used in the present study is similar to that used in the study performed by Jiang et al. [29] thus the parameters for material definition were selected considering the results from that study. In ABAQUS, the viscoelastic (VE) and hyperplastic properties of rubber material are usually modeled separately. Mooney–Rivlin model and/or Yeoh model can be used to simulate the constitutive model of rubber. In theory, the Mooney–Rivlin model is preferable for strain amplitude ranging from 20% to 150% whereas the Yeoh model is suitable for strain amplitudes greater than 150% [16]. This principle is considered in this research with the adopted parameters for modeling the rubber shown in Table 3. As mentioned before, this study assumes that rubber is an incompressible and isotropic material, and thus D_1, parameter determined by the compressibility of the material is set to 0. The parameters describing the shear behavior C_{10} and C_{01} are fitted according to the data from the previously mentioned study [29]. Since the VE materials exhibit creep under constant stress and stress relaxation under constant strain, the Prony series is used to describe the VE behavior. The associated parameters needed to be defined in the Prony series are the shear modulus (*g–i Prony*), the bulk modulus (*k–i Prony*), and the relaxation time (*tau–i Prony*). The values adopted for these parameters are also shown in Table 3. The steel plates adopted a nominal strength of 345 MPa corresponding to steel Q345, one kind of Chinese standardized mild steel.

5.2. Simulated Results. In Figure 15 the test results and the simulated results are compared. It can be seen that the numerical simulation using the parameters presented in Table 3 predicts correctly the behavior of MLVED. However, for 30 mm, amplitude corresponding to 300% strain, the test results are slightly unsymmetrical for tension and compression loading due to the various conditions of the physical setup such as the self-weighs of the specimen and the actuator. Consequently, experimental results show some differences with respect to the numerical simulations in terms of maximum damping force in one loading direction. Furthermore, the simulated results are smoother and more ideal if compared with those of the test. Nevertheless, the overall agreement between the results may be considered satisfactory.

Table 4: Comparison between model results and experimental results.

Strain (%)	Damping force (kN)			Loss factor			Storage modulus (MPa)			Loss modulus (MPa)		
	Test	Model	Error (%)	Test	Model	Error (%)	Test	Model	Error (%)	Test	Model	Error (%)
25	113	108	4.18	0.34	0.33	4.41	1.07	1.02	4.61	0.36	0.34	6.49
50	176	190	8.18	0.32	0.35	10.0	0.92	0.85	7.23	0.29	0.27	7.28
75	220	235	6.73	0.26	0.28	6.06	0.78	0.75	3.51	0.21	0.22	4.76
100	301	311	3.51	0.27	0.26	2.62	0.72	0.75	4.62	0.19	0.20	4.58
125	322	350	8.78	0.23	0.25	10.13	0.70	0.63	10.16	0.16	0.18	12.36
150	411	418	1.64	0.21	0.22	1.90	0.69	0.67	2.60	0.15	0.16	3.33
200	510	525	2.89	0.20	0.21	2.94	0.65	0.63	2.49	0.13	0.14	3.73
250	648	657	1.28	0.18	0.17	2.86	0.64	0.66	2.56	0.11	0.10	2.80
300	778	851	9.31	0.14	0.16	10.71	0.66	0.72	9.37	0.09	0.11	13.51
	Equivalent stiffness (kN/mm)			Equivalent damping (kN·s/mm)			Equivalent damping ratio			Dissipated energy (N·mm)		
	Test	Model	Error (%)	Test	Model	Error (%)	Test	Model	Error (%)	Test	Model	Error (%)
25	38.4	36.7	4.50	2.08	1.99	4.46	0.200	0.189	5.50	35.04	33.45	4.54
50	32.9	29.8	9.64	1.67	1.53	8.33	0.188	0.173	7.98	129.92	118.46	8.82
75	28.0	27.0	3.51	1.18	1.22	3.57	0.181	0.172	4.97	147.20	155.95	5.95
100	25.9	27.1	4.62	1.10	1.15	4.45	0.173	0.181	4.62	235.17	246.34	4.75
125	25.3	22.80	10.17	0.92	1.02	11.11	0.166	0.183	10.24	323.51	359.34	11.07
150	24.9	23.58	5.35	0.84	0.86	2.99	0.159	0.165	3.77	411.20	425.02	3.36
200	23.2	22.43	3.56	0.75	0.78	3.45	0.156	0.149	4.49	628.68	648.76	3.19
250	23.5	22.93	2.74	0.66	0.64	2.44	0.145	0.139	4.14	849.89	820.00	3.52
300	23.7	25.87	9.16	0.53	0.60	13.58	0.124	0.112	9.68	1,085.02	1,184.55	9.17

Mechanical performance index comparison including damping force, loss factor, storage modulus, loss modulus, equivalent stiffens, equivalent damping, and dissipated energy is summarized in Table 4. Although the slope and area of force–displacement curves of the model are in good agreement with those of the test as shown in Figure 15, it is important to note that during the test, for some loading cases unsymmetrical maximum amplitudes were applied due to various conditions from the physical setup. Consequently, the average difference between the mechanical performance index of the test and the model is slightly considerable. However, the overall average difference considering all indexes together is about 5.67%.

6. Numerical Evaluation of Mechanical Properties Variation of MLVED for Different VE Layers Sizes

6.1. Models Description. Aiming to evaluate the properties of the MLVED considering different sizes, five additional models of the specimen were created. Four of them used the same layout configuration and parameters of those from the specimen however with different sizes and thickness. The last one was modeled with only two VE layers aiming to state how much space (in the area) is saved by using four VE layers to reach the same level of damping force instead of the traditional two VE layers. The models are named ML-A, ML-B, ML-C, ML-D, and ML-E with the first four having four VE layers each with the area and thickness of $200 \times 200 \times 10$, $500 \times 500 \times 10$, $300 \times 300 \times 8$, and $300 \times 300 \times 15$, respectively. The main objective is to evaluate the variation of the mechanical properties of the MLVED if different VE layers areas and thicknesses are considered. The last model has two VE layers with area and thickness of $600 \times 600 \times 10$. This area was set by trial calculations considering that the same damping force of the specimen should be reached. For better accuracy of the results, the model created in Section 5 (calibrated model) was used as the reference model instead of the tested specimen. By this approach, the parameters of the VE material were kept constant to simulate exactly the same material properties. The loading protocol was applied considering the same strain amplitude used during the test and the detailed displacement amplitude for each MLVED is presented in Table 5.

6.2. Simulated Results. The resulting force–displacement curves of simulated MLVED with different VE layers sizes and thicknesses are presented in Figure 16. From the graphs, it can be observed that for all considered dimensions of MLVEDs under all considered strain amplitudes, the stress–strain curves form hysteresis loops, indicating the effective energy dissipation during cyclic loadings. For strain amplitudes smaller than 80%, the hysteresis loop is a smooth ellipse showing a typical behavior for linear VE materials. When the strain amplitude is greater than 80% the hysteresis loop shows a hardening effect indicating that the stiffness and damping increase with the increment of strain amplitude. The energy dissipation capacity follows the same trend given that the slope and area of strain–force curves increase with the strain amplitude. However, the maximum damping force varies according to the sizes of MLVEDs. Taking C-M as a reference, the influence of both area and

Table 5: Loading protocol for simulation of different MLVED sizes.

Damper	Displacement (mm)	Strain amplitude (%)
CM	2.5, 5.0, 7.5, 10.0, 12.5, 15.0, 20.0 25.0, 30.0	25, 50, 75, 100, 125, 150, 200 250, 300
ML-A	2.5, 5.0, 7.5, 10.0, 12.5, 15.0, 20.0 25.0, 30.0	25, 50, 75, 100, 125, 150, 200 250, 300
ML-B	2.5, 5.0, 7.5, 10.0, 12.5, 15.0, 20.0 25.0, 30.0	25, 50, 75, 100, 125, 150, 200 250, 300
ML-C	2.0, 4.0, 6.0, 8.0, 10.0, 12.0, 16.0 20.0, 24.0	25, 50, 75, 100, 125, 150, 200 250, 300
ML-D	3.75, 7.50, 11.25, 15.0, 18.75, 22.50, 30.0 37.5, 45.0	25, 50, 75, 100, 125, 150, 200 250, 300
ML-E	2.5, 5.0, 7.5, 10.0, 12.5, 15.0, 20.0 25.0, 30.0	25, 50, 75, 100, 125, 150, 200 250, 300

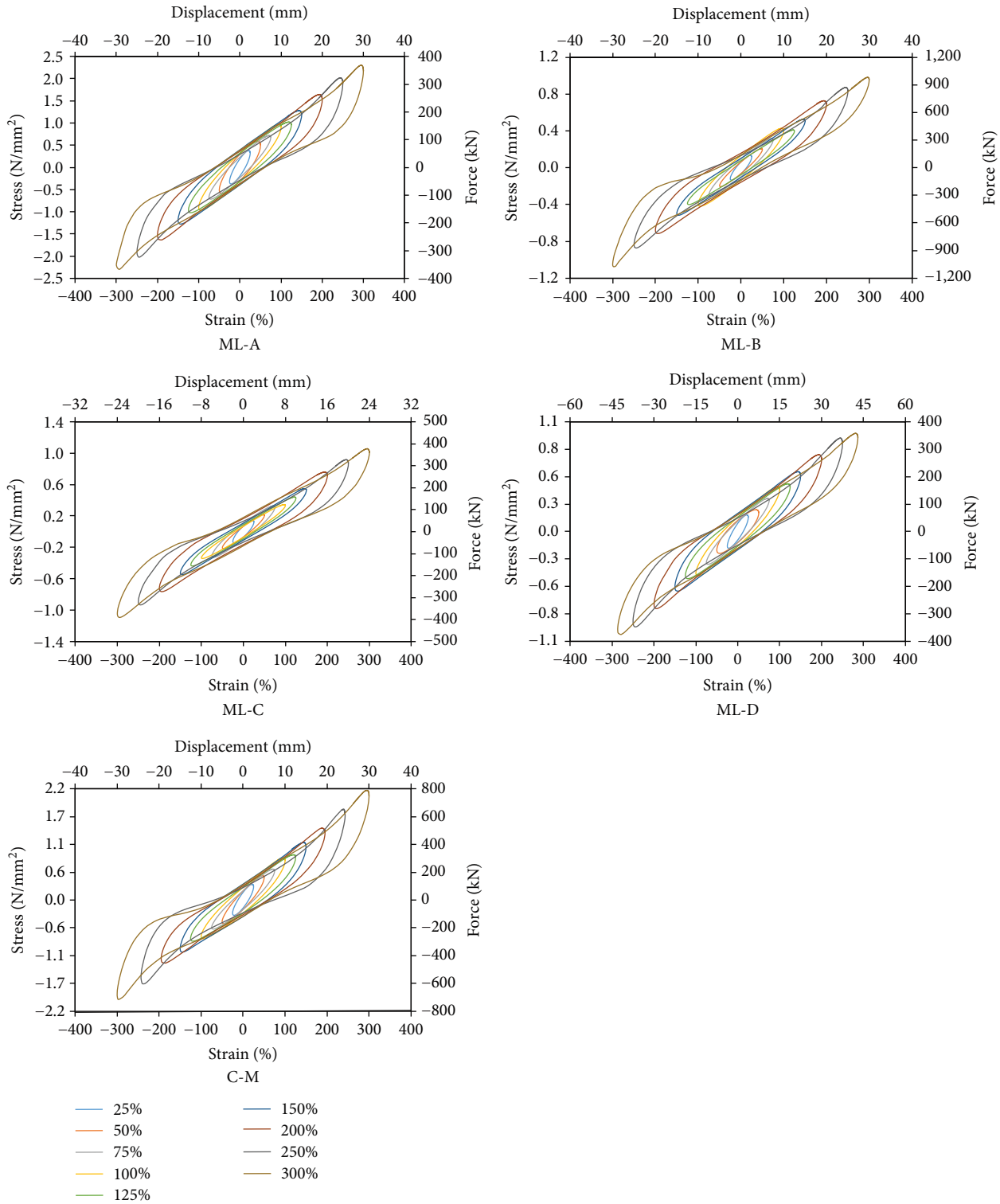

Figure 16: Hysteresis curves of MLVEDs with different VE layers sizes and thickness.

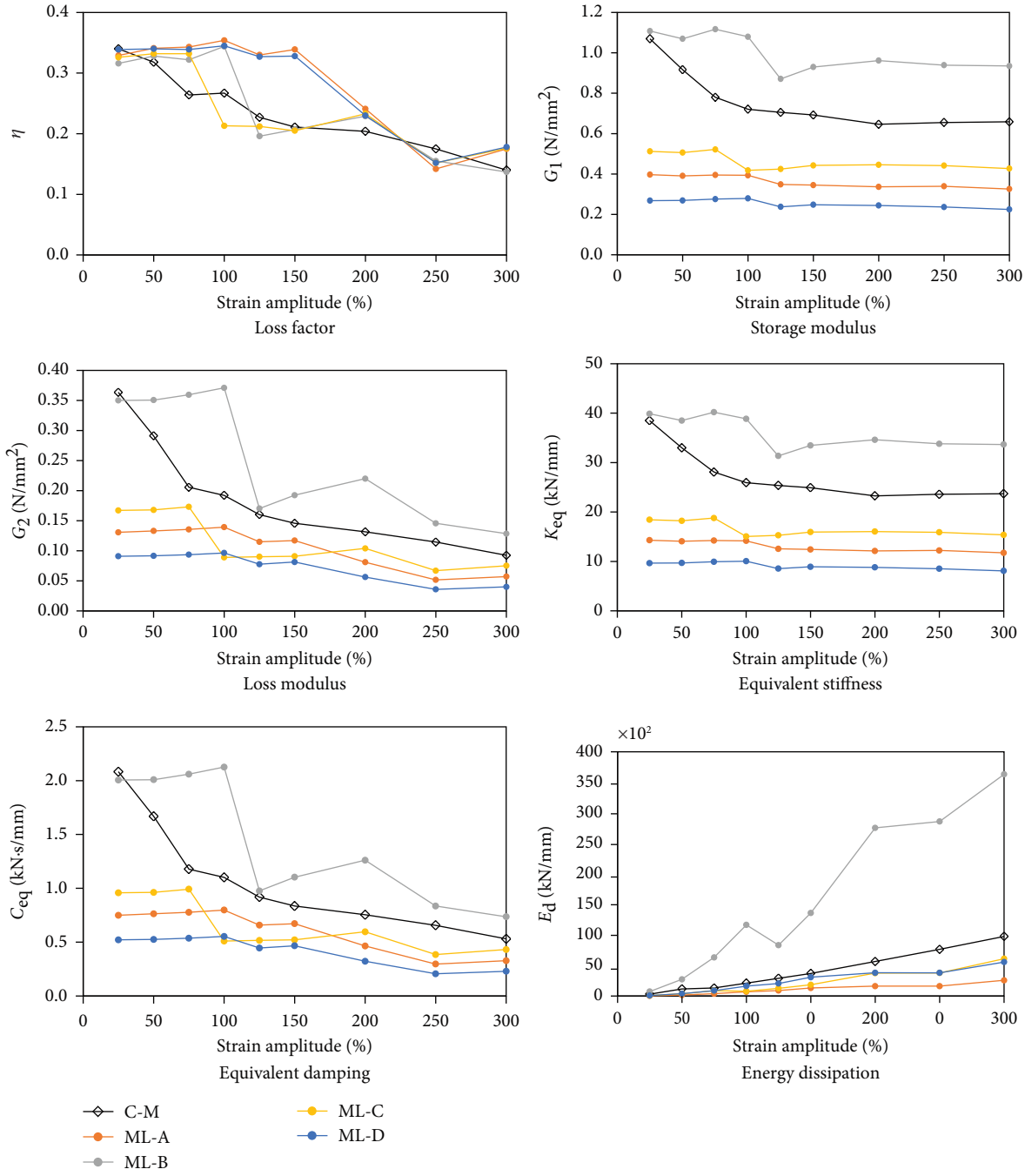

Figure 17: Dynamic parameters change with strain for different VE layers sizes and thickness.

thickness variation within VE layers was observed. The maximum observed damping force was about 400, 800, and 1,000 kN for ML-A, C-M, and ML-B, respectively, confirming that a greater VE layer area results in higher damping forces. A different scenario is observed for thickness variation. Reducing the thickness from 10 (C-M) to 8 mm (ML-C) the maximum damping force was reduced from 800 to 400 kN, the same behavior when the thickness was increased from 10 (C-M) to 15 mm (ML-D). This variation shows that the relationship between the energy dissipation capacity and the thickness is not linear, and thus is of crucial importance to select the appropriate thickness considering the area of the VE layer.

The influence of VE layer area and thickness variation on the mechanical properties of MLVED was also investigated by analyzing the damping force, loss factor, storage modulus, loss modulus, equivalent stiffens, equivalent damping, and energy dissipation for different MLVED sizes and strain amplitudes (shown in Figure 17). All the dampers follow the same trend regardless of the VE layers' size and thickness. When strain

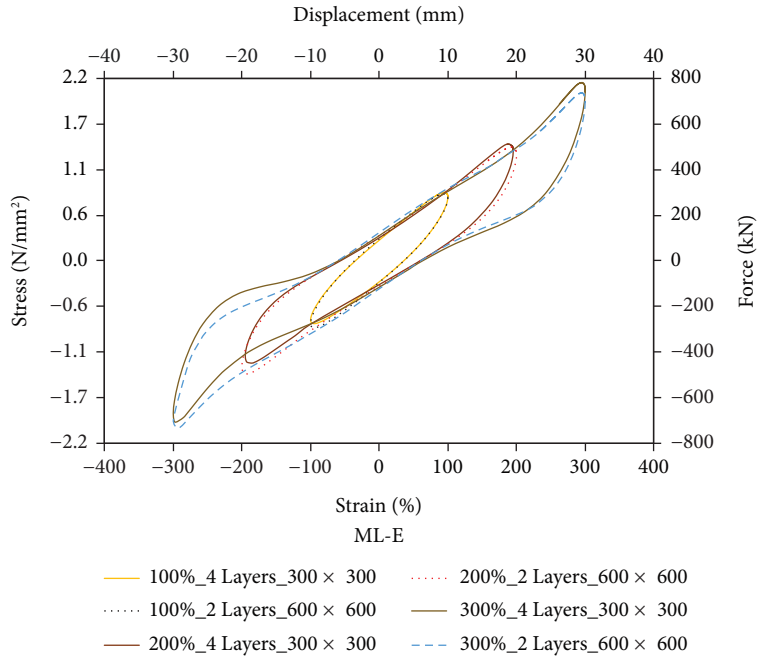

Figure 18: Hysteresis curves comparison between four and two layers VED with 300 × 300 and 600 × 600 mm, respectively.

amplitude increases the loss factor reduces gradually for all the dampers except for ML-B on which the loss factor shows an abrupt variation from 100% to 200% strain. The storage modulus and equivalent stiffness showed less influence of strain amplitude, especially for amplitudes greater than 125%; however, these indices for C-M and ML-B show a slight reduction for amplitudes lower than 120%. The loss modulus and equivalent damping showed to have a reduction relationship with strain amplitude for all dampers except ML-B on which zero correlation was observed. For energy dissipation, all dampers showed to have approximately a linear increase relationship with the strain amplitude except ML-B on which the increment is not linear.

As mentioned before, aiming to state how much space is saved by using four VE layers instead of the traditional two, another model of the specimen (ML-E) was created. Compared to the reference model, this model needs to be 270,000 mm^2 larger to reach the same damping force performance as the reference one. This additional area is not beneficial when the available space to install the dampers is reduced. The resulting force–displacement curves of this model were compared to those from the reference model for 100%, 200%, and 300% strain amplitudes, respectively, and shown in Figure 18. It can be observed that the slope and enveloping area remains almost the same showing that the increment of the area of VE layers is proportional to the increase of the corresponding damping force.

7. Conclusions and Recommendations

Traditional VEDs consist of two rectangular VE layers bounded between three rectangular steel plates on which the energy dissipation originates from the inherent shear deformation of the VE layers. This design concept has been proven to be very effective if the damper is well installed. However, if larger damping forces are needed, the size of the damper (the shear area of VE layers) has to be increased. Two main issues are associated with this large area. First, the steel plates are more susceptible to experiencing buckling due to out-of-plane deformations. Second, the overall size of the damper becomes larger which is not desirable from the architectural perspective and sometimes from the space usage perspective. Accounting for these two limitations, in the present study, an innovative VED so-called MLVED is proposed and investigated both numerically and experimentally. The proposed MLVED consists of four rectangular VE layers bounded between five rectangular steel plates, two outer plates, and three at the center. The damper was subjected to cyclic loading tests to investigate its dynamic mechanical performance and numerical models proposed by previous researchers were adopted to simulate the hysteretic behavior of the proposed MLVED. The following includes the main outcomes of the present research:

(1) The proposed MLVED proved to have excellent energy dissipation capacity since the force–displacement curves obtained from the test form full and stable hysteretic loops, indicating effective energy dissipation during cyclic loading;

(2) The proposed MLVED is effective in dissipating energy at all levels of vibration which further promotes its application under different loading conditions;

(3) The device is not sensitive to frequency since all the mechanical properties remained stable for different loading frequencies;

(4) The slope and enveloping area increased obviously with the increase of strain amplitude showing that

the MLVED is highly strain dependent with hardening of the VE material starting at amplitudes larger than 80% strain;

(5) The MLVED showed to have excellent antifatigue performance since the properties of the damper remained stable after 30 cycles of loading with the deterioration of the mechanical properties less than 9%;

(6) The MLVED showed to be beneficial when the space to install the dampers is reduced since by using MLVED 270,000 mm^2 of the total area occupied by the damper can be saved;

(7) The MLVED showed to be temperature dependent. However, the energy dissipation capacity remains stable;

(8) The dynamic mechanical properties of the MLVED fluctuate with the increase of strain amplitude showing a decrease in storage modulus, loss modulus, and the loss factor, especially for strain amplitudes less than 100%;

(9) The numerical analysis results showed the Mooney–Rivlin model, the Yeoh model, and the Prony series can be used to accurately predict the behavior of the proposed MLVED within their applicable strain range;

(10) Numerical simulations have also shown that area size and thickness variation of VE layers have a great influence on the mechanical properties and energy dissipation capacity of the MLVED. However, this variation showed to have a nonproportional correlation with the damper performance, and thus is of crucial importance to select the appropriate thickness considering the area of the VE layer.

This paper investigates the mechanical proprieties of the proposed MLVED considering an experimental full test of one specific size MLVED. To fully understand the effect of VE layers area size and thickness variation, further experimental studies are required to verify the results obtained from numerical investigations. In addition, some innovative tools such as the ones used in previous studies [30–32] are suggested to be used in extension to this study.

Data Availability

The data used to support the findings of this study are available from the corresponding author upon request.

Conflicts of Interest

The authors declare that they have no conflicts of interest.

Acknowledgments

The authors gratefully acknowledge the financial support from the National Natural Science Foundation Project of China (Grant no. 52025083) and the Shanghai Science and Technology Innovation Action Plan (Grant no. 22dz1201400).

References

[1] H. Li, T. Yi, M. Gu, and L. Huo, "Evaluation of earthquake-induced structural damages by wavelet transform," *Progress in Natural Science*, vol. 19, no. 4, pp. 461–470, 2009.

[2] Q. Yang, R. Gao, F. Bai, T. Li, and Y. Tamura, "Damage to buildings and structures due to recent devastating wind hazards in East Asia," *Natural Hazards*, vol. 92, no. 3, pp. 1321–1353, 2018.

[3] Y. Zhou, X. Lu, D. Weng, and R. Zhang, "A practical design method for reinforced concrete structures with viscous dampers," *Engineering Structures*, vol. 39, pp. 187–198, 2012.

[4] X. Chen, C. Li, and J. Tang, "Structural integrity of wind turbines impacted by tropical cyclones: a case study from China," in *Journal of Physics: Conference Series*, IOP Publishing, 2016.

[5] Z. Li, S. Chen, H. Ma, and T. Feng, "Design defect of wind turbine operating in typhoon activity zone," *Engineering Failure Analysis*, vol. 27, pp. 165–172, 2013.

[6] G. W. Housner, L. A. Bergman, T. K. Caughey et al., "Structural control: past, present, and future," *Journal of Engineering Mechanics*, vol. 123, no. 9, pp. 897–971, 1997.

[7] T. T. Soong and B. F. Spencer, "Supplemental energy dissipation: state-of-the-art and state-of-the-practice," *Engineering Structures*, vol. 24, no. 3, pp. 243–259, 2002.

[8] O. A. Marzouk and A. H. Nayfeh, "Control of ship roll using passive and active anti-roll tanks," *Ocean Engineering*, vol. 36, no. 9-10, pp. 661–671, 2009.

[9] H. Li, S.-Y. Wang, G. Song, and G. Liu, "Reduction of seismic forces on existing buildings with newly constructed additional stories including friction layer and dampers," *Journal of Sound and Vibration*, vol. 269, no. 3–5, pp. 653–667, 2004.

[10] F. Boggian, A. Aloisio, and R. Tomasi, "Experimental and analytical study of friction connection for seismic retrofit with cross-laminated timber (CLT) panels," *Earthquake Engineering & Structural Dynamics*, vol. 51, no. 14, pp. 3304–3326, 2022.

[11] J. M. Tchamo and Y. Zhou, "An alternative practical design method for structures with viscoelastic dampers," *Earthquake Engineering and Engineering Vibration*, vol. 17, no. 3, pp. 459–473, 2018.

[12] C. Keel and P. Mahmoodi, "Design of viscoelastic dampers for Columbia Center Building," in *Building Motion in Wind*, ASCE, 1986.

[13] P. Mahmoodi and C. Keel, "Performance of viscoelastic structural dampers for the Columbia Center Building," in *Building Motion in Wind*, ASCE, 1986.

[14] K. C. Chang, T. T. Soong, S.-T. Oh, and M. L. Lai, "Seismic behavior of steel frame with added viscoelastic dampers," *Journal of Structural Engineering*, vol. 121, no. 10, pp. 1418–1426, 1995.

[15] Z.-D. Xu, C. Xu, and J. Hu, "Equivalent fractional Kelvin model and experimental study on viscoelastic damper," *Journal of Vibration and Control*, vol. 21, no. 13, pp. 2536–2552, 2015.

[16] Y. Chen, C. Chen, Q. Ma, H. Jiang, and Z. Wan, "Study on mechanical properties of high damping viscoelastic dampers," *Advances in Structural Engineering*, vol. 22, no. 14, pp. 2925–2936, 2019.

[17] M. Han, R. Twizeyimana, and H. Du, "Experimental study on mechanical properties of small size viscoelastic damper," in *E3S Web of Conferences*, EDP Sciences, 2021.

[18] Z.-D. Xu, T. Ge, and J. Liu, "Experimental and theoretical study of high-energy dissipation-viscoelastic dampers based

on acrylate-rubber matrix," *Journal of Engineering Mechanics*, vol. 146, no. 6, Article ID 04020057, 2020.

[19] M. Montgomery and C. Christopoulos, "Experimental validation of viscoelastic coupling dampers for enhanced dynamic performance of high-rise buildings," *Journal of Structural Engineering*, vol. 141, no. 5, Article ID 04014145, 2015.

[20] Z. Shu, B. Ning, S. Li, Z. Li, Z. Gan, and Y. Xie, "Experimental and numerical investigations of replaceable moment-resisting viscoelastic damper for steel frames," *Journal of Constructional Steel Research*, vol. 170, Article ID 106100, 2020.

[21] D. M. Osabel, D. Sato, and K. Kasai, "Experimental study of a brace-type viscoelastic," *Earthquake Engineering*, vol. 31, pp. 1511–1528, 2020.

[22] C. Fang, Y. Ping, Y. Chen, M. C. H. Yam, J. Chen, and W. Wang, "Seismic performance of self-centering steel frames with SMA-viscoelastic hybrid braces," *Journal of Earthquake Engineering*, vol. 26, no. 10, pp. 5004–5031, 2022.

[23] H. Qian, D. Wei, Y. Shi, Z. Li, and H. Li, "Pre-tensioned SMA cable tests and its application in a novel self-centering viscoelastic damper," *Soil Dynamics and Earthquake Engineering*, vol. 168, Article ID 107850, 2023.

[24] X. Fang, Y. Zhou, K. Bi, H. Hao, and T. Wang, "Experimental study on the cyclic behaviors of an innovative lead-viscoelastic coupling beam damper (LVCBD)," *Journal of Building Engineering*, vol. 64, Article ID 105596, 2023.

[25] R.-H. Zhang, T. T. Soong, and P. Mahmoodi, "Seismic response of steel frame structures with added viscoelastic dampers," *Earthquake Engineering & Structural Dynamics*, vol. 18, no. 83, pp. 389–396, 1989.

[26] Z. D. Xu, Y. X. Liao, T. Ge, and C. Xu, "Experimental and theoretical study of viscoelastic dampers with different matrix rubbers," *Journal of Engineering Mechanics*, vol. 142, no. 8, Article ID 04016051, 2016.

[27] JG/T 209-2012, *Dampers for Vibration Energy Dissipation of Building*, China Standard Press, Beijing, 2012.

[28] ABAQUS, *Analysis User's Manual, Version 6.14*, Dassault Systemes Simulia Corporation, 2014.

[29] H. Jiang, S. Li, and L. He, "Experimental study on a new damper using combinations of viscoelastic material and low-yield-point steel plates," *Frontiers in Materials*, vol. 6, Article ID 100, 2019.

[30] G. C. Marano, M. M. Rosso, and J. Melchiorre, "Optimization as a tool for seismic protection of structures," in *World Conference on Seismic Isolation*, pp. 100–113, Springer International Publishing, Cham, 2022.

[31] G. Devillanova and G. C. Marano, "A free fractional viscous oscillator as a forced standard damped vibration," *Fractional Calculus and Applied Analysis*, vol. 19, no. 2, pp. 319–356, 2016.

[32] G. C. Marano, F. Trentadue, and R. Greco, "Stochastic optimum design criterion of added viscous dampers for buildings seismic protection," *Structural Engineering and Mechanics*, vol. 25, no. 1, pp. 21–37, 2007.